www.sciencemag.org/cgi/content/full/1176088/DC1

Supporting Online Material for

Structure and Mechanism of a Na^+-Independent Amino Acid Transporter

Paul L. Shaffer, April Goehring, Aruna Shankaranarayanan, Eric Gouaux*

*To whom correspondence should be addressed. E-mail: gouauxe@ohsu.edu

Published 16 July 2009 on *Science* Express
DOI: 10.1126/science.1176088

This PDF file includes:

Table of Contents

Materials and Methods

Protein purification. The MJ0609 (ApcT) protein was discovered as a stable species suitable for crystallographic studies by application of fluorescence-detection size exclusion chromatography (FSEC) (*1*) method and was overexpressed in *Escherichia coli* C41 cells (*2*) as a carboxyl terminal fusion with a variant of green fluorescent protein (GFPuv) (*3-6*) following induction by isopropyl-β-D-thiogalactoside (IPTG) at 20°C. Cells were lysed using an Avestin homogenizer, the resulting membranes solubilized by *n*-dodecyl-β-D-maltoside and the protein purified by metal ion affinity chromatography. GFP was removed by thrombin digestion and the ApcT protein was further purified by size exclusion chromatography (SEC) in *n*-octyl-β-D-thioglucoside (C_8SG). The murine monoclonal antibody 7F11 (IgG) was generated by standard methods (*7*) and purified from hybridoma supernatant by ion exchange chromatography. The Fab fragment was prepared by proteolytic cleavage with papain and purified by ion exchange chromatography. The ApcT – 7F11 Fab complex was formed by mixing components at a stoichiometric ratio of 1:1.2, respectively, and was isolated by SEC in C_8SG. Selenomethionine (SeMet)-labeled transporter protein (*8*) was prepared as previously described and purified like wild-type protein.

Cloning of 7F11 Fab genes. Total RNA (1μg) isolated from 1 x 10^7 7F11 hybridoma cells was used as the template for first strand synthesis and subsequent 5' rapid amplification of cDNA ends (RACE; Clontech) according to the manufacturer's instructions. Gene-specific primers were used to clone the IgG2b heavy chain Fab portion (5'-GCT GTG TGT ACT TCC ACG TTG TTC ACA AAC CAG C-3') and the kappa light chain (5'-GAG CTG GGG AGC

TGG TGG TGG CAT CTC-3') (*9*). The 5' RACE products were cloned into a TA vector (Invitrogen) and both strands were sequenced.

Crystallization. Isolated ApcT and its Fab complex were crystallized under paraffin oil at 20°C. Initial hits were identified using the Hauptman-Woodward Institute high throughput screening facility. Well diffracting crystals of ApcT grew when ApcT at about 5-10 mg/ml in 10 mM Tris (pH 8.0), 50 mM NaCl, and 20 mM C_8SG was mixed 1:1 with drop solution containing 100 mM Bicine (pH 9.0), 100 mM NaCl and 39-45% PEG 550 MME in the presence of either mercury (mercury acetate, PCMB, or thimerosal) or holmium salts ($HoCl_3$). Crystals of the Fab complex also grew under oil by microbatch method under a wide variety of pH, salt, and PEG conditions. The data sets used in this study were collected from crystals of: SeMet ApcT – 7F11 Fab grown in 100 mM Bicine (pH 9.0), 100 mM KH_2PO_4, and 37-43% PEG 550 MME; wt ApcT – 7F11 Fab grown in 100 mM sodium acetate (pH 5.0), 100 mM RbCl, 100 mM L-Ala and 40-48% PEG 400; and ApcT K158A – 7F11 Fab grown in 100 mM sodium acetate (pH 5.0), 100 mM $NH_4H_2PO_4$, and 40-44% PEG 400.

Data collection and structure determination. Crystals were harvested through the paraffin oil and directly cooled in liquid nitrogen. All diffraction data was collected at 100K using synchrotron radiation at the Advanced Light Source (ALS; beamlines 8.2.1, 8.2.2, and 5.0.2). Diffraction data sets were indexed and scaled using HKL2000 (*10*). Initial phases for the ApcT –Fab complex were derived by combining experimental phases (SigmaA; CCP4 computer program suite) (*11, 12*) from SeMet-labeled ApcT and calculated phases from a molecular replacement solution (*13*) using a Fab search probe (Phaser) (*14*). Manual building of the majority of the transmembrane helices yielded a molecular replacement probe that was used to

solve the structure of the isolated, non Fab bound transporter. The resulting molecular replacement phases enabled rapid and nearly complete autobuilding by Arp/Warp (*15*). The structures were refined by iterative cycles of refinement and manual rebuilding using Refmac (*16*) and Coot (*17*). Structure validation was done using Procheck (*18*) and MolProbity (*19*). All figures were prepared using Pymol (*20*).

ApcT Reconstitution and radioligand uptake assays. Liposomes were prepared using a 3:1 ratio of *E. coli* total lipid extract to chicken egg phosphatidylcholine in 20 mM HEPES-Tris pH 7.4, 100 mM Choline Cl (Avanti Polar Lipids). An extruder was used to obtain unilamellar vesicles and the preformed liposomes were treated with Triton X-100 at a 2.5:1 (w:w) lipid to detergent ratio. Purified ApcT was reconstituted at a protein to lipid ratio of 1:110 and excess detergent was removed by adsorption onto Bio-Beads and proteoliposomes were frozen at -80°C for storage until needed. Unless indicated otherwise, proteoliposomes were loaded with 25 mM citrate/phosphate buffer at desired pH, 100 mM NaCl, and 4 mM L-Ala. Transport was initiated by adding liposomes to reaction buffer containing 25 mM citrate/phosphate at desired pH, 100 mM NaCl, and 500 nM [^{3}H]-L-Ala at 30°C. For the competition experiment, proteoliposomes were loaded with 25 mM citrate/phosphate buffer (pH 4.0), 100 mM NaCl, 4 mM L-Ala and the reaction buffer contained 25 mM citrate/phosphate buffer (pH 4.0), 100 mM NaCl, 500 nM [^{3}H]-L-Ala and 10 mM of indicated cold competitor. Reactions were terminated after 20 minutes, proteoliposomes isolated by filtration through nitrocellulose filters, and uptake quantitated by scintillation counting.

Measurement of inter-helical angles. The scaffold helices (TMs 3-5, 8-10 LeuT numbering) of Apct, vSGLT (PDB ID: 3DH4), Mhp1 (2JLN) and BetP (2W8A) were

superposed on that of LeuT (2A65) using the DaliLite pairwise structural superposition (*21*) with a RMSD of 2.8 Å, 3.4 Å, 2.3 Å and 2.8 Å for Cα atoms, respectively and the relative difference in the orientations of TMs1 and 6 were analyzed using the interhlx program (K. Yap, University of Toronto). In particular, the angle between TM1a (or TM1b) helices of ApcT, vSGLT, Mhp1 and BetP with reference to LeuT was calculated using the interhlx program. The helical axis was defined based on the following residue boundaries for TM1a (Leu T: 10-20, ApcT: 10-20, vSGLT: 53-63, Mhp1: 28-38 and BetP: 138-148) and TM 1b (LeuT: 25-37, ApcT: 29-37, vSGLT: 67-78, Mhp1: 43-55 and BetP: 152-168). Sign conventions for the interhelical angles are as described before (*22*). TMs 1-10 of ApcT superimpose with that of LeuT, SGLT, MhP1 and BetP with a RMSD of 3.4 Å, 3.7 Å, 3.9 Å and 3.7 Å, respectively.

GenBank accession numbers. GenBank accession numbers of the transporters to generate the Dendrogram in Fig. 1A and the alignments in Figs. 3C and 4A are as follows: ApcT gi|1591319, PotE gi|77416694, AdiC gi|38605621, LysP gi|34395946, GabP gi|120778, AroP gi|32172425, PheP gi|130068, LeuT gi|15607041, GNP1 gi|1708002, CAN1 gi|729014, SLC7A1 gi|4507047, SLC7A2 gi|85397783, SLC7A3 gi|57162668, SLC7A4 gi|47678691, SLC7A5 gi|12643412, SLC7A6 gi|117167801, SLC7A7 gi|4581435, SLC7A8 gi|4581470, SLC7A9 gi|24020985, SLC7A10 gi|9790235, SLC7A11 gi|5668545, SLC7A13 gi|116284086**,** SLC12A1 gi|134254459**,** SLC12A2 gi|1709292**,** SLC12A3 gi|223634707, SLC12A4 gi|27151691**,** SLC12A5 gi|161784306**,** SLC12A6 gi|27151690**,** SLC12A7 gi|166202480**,** SLC32A1 gi|29428257**,** SLC36A1 gi|41352721**,** SLC36A2 gi|222418631**,** SLC36A3 gi|222446642**,** SLC36A4 gi|40807351**,** SLC38A1 gi|117168277**,** SLC38A2 gi|48146651**,** SLC38A3 gi|5870893**,** SLC38A4 gi|31543737**,** SLC38A5 gi|193788624.

Dendrogram calculation (Fig. 1). The tree was generated with TreeView (*23*) from an alignment done with ClustalW (*24*). Branches corresponding to prokaryotic APCs, CATs, CCCs, VIATT, SNATs, PATs and HATs are defined in Table S1. The scale bar represents 0.1 substitutions per amino acid position.

Calculation of pKa values. The pKa of Lys158 was calculated using PROPKA (http://propka.ki.ku.dk/)(*25*)

References

1. T. Kawate, E. Gouaux, *Structure* **14**, 673 (2006).
2. B. Miroux, J. Walker, *J. Mol. Biol.* **260**, 289 (1996).
3. J. G. Morin, J. W. Hastings, *J. Cell Physiol.* **77**, 313 (1971).
4. H. Morise, O. Shimomura, F. H. Johnson, J. Winant, *Biochemistry* **13**, 2656 (1974).
5. M. Chalfie, Y. Tu, G. Euskirchen, W. W. Ward, D. C. Prasher, *Science* **263**, 802 (1994).
6. J. Zhang, R. E. Campbell, A. Y. Ting, R. Y. Tsien, *Nat. Rev. Mol. Cell Biol.* **3**, 906 (2002).
7. E. Harlow, D. Lane, *Antibodies: A Laboratory Manual* (Cold Spring Harbor Laboratory Press, Cold Spring Harbor, 1989), pp.
8. W. A. Hendrickson, J. R. Horton, D. M. LeMaster, *EMBO J.* **9**, 1665 (1990).
9. P. S. Shepherd, C. J. Dean, Eds., *Monoclonal Antibodies: A Practical Approach* (Oxford University Press, New York, NY, 2000), pp.
10. Z. Otwinowski, W. Minor, *Meth. Enzymol.* **276**, 307 (1997).
11. N. *CCP4* Project, *Acta Crystallogr.* **D50**, 760 (1994).
12. E. Potterton, P. Briggs, M. Turkenburg, E. Dodson, *Acta Crystallogr. D.* **59**, 1131 (2003).
13. M. G. Rossmann, *Acta Crystallogr. A.* **46**, 73 (1990).
14. A. J. McCoy, R. W. Grosse-Kunstleve, L. C. Storoni, R. J. Read, *Acta Crystallogr. D.* **61**, 458 (2005).
15. G. Langer, S. X. Cohen, V. S. Lamzin, A. Perrakis, *Nat. Protoc.* **3**, 1171 (2008).
16. G. N. Murshudov, A. A. Vagin, E. J. Dodson, *Acta Crystallogr. D.* **53**, 240 (1997).
17. P. Emsley, K. Cowtan, *Acta Crystallogr. D.* **60**, 2126 (2004).
18. R. A. Laskowski, M. W. MacArthur, D. S. Moss, J. M. Thornton, *J. Appl. Crystallogr.* **26**, 283 (1993).
19. I. W. Davis *et al.*, *Nucleic Acids Res.* **35**, W375 (2007).
20. W. L. DeLano. (DeLano Scientific, San Carlos, CA, USA, 2002).
21. L. Holm, J. Park, *Bioinformatics* **16**, 566 (2000).
22. A. C. Drohat *et al.*, *Biochemistry* **35**, 11577 (1996).
23. R. D. M. Page, *Comp. Appl. Biosci.* **12**, 357 (1996).
24. J. D. Thompson, D. G. Higgins, T. J. Gibson, *Nucleic Acids Res.* **22**, 4673 (1994).
25. H. Li, A. D. Robertson, J. H. Jensen, *Proteins* **61**, 704 (2005).

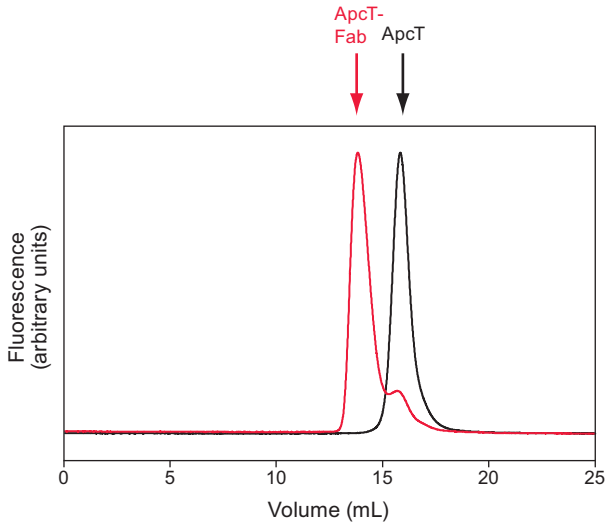

Fig. S1. Size exclusion chromatography elution profile of ApcT alone (black) and ApcT-7F11 Fab complex (red). Samples solubilized in n-octyl-ß-d-thioglucoside (C8SG) were injected onto a Superdex 200 column and monitored by tryptophan fluorescence.

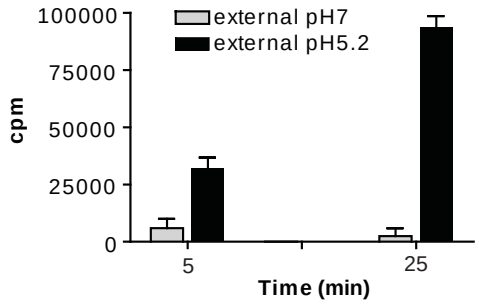

Fig. S2. [^{3}H] Ala counterflow requires a low pH. [^{3}H]Ser, [^{3}H]Gln, [^{3}H]Ala, and [^{3}H]Gly uptake by ApcT reconstituted into lipid vesicles. Proteoliposomes were loaded with 20mM Hepes/Tris pH7, 100mM NaCl, + 4mM Ala, 4mM Gln, 4mM Ser, and 4mM Gly. Uptake was performed at 30°C in either 20mM Hepes/Tris pH7, 100mM NaCl or 20mM Hepes pH5.2, 100mM NaCl and in the presence of 500nM (each) [^{3}H]serine, [^{3}H]glutamine, [^{3}H]alanine, and [^{3}H]glycine. Time points were taken at 5 and 25 min. Background was defined as no protein loaded into the proteoliposomes. Error bars represent SEM of triplicate measurements.

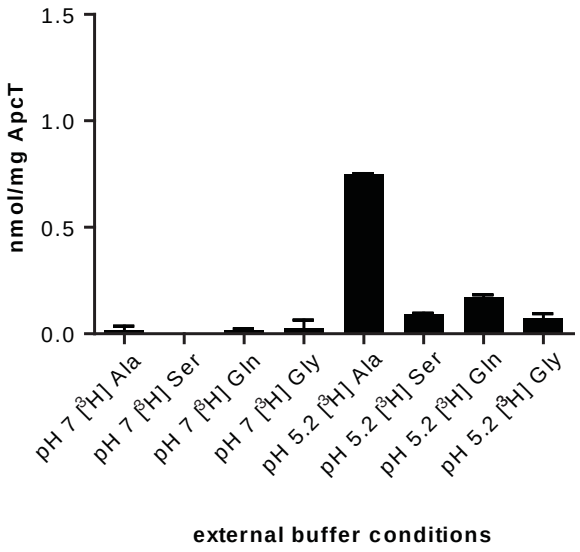

Fig. S3. Ala is the most efficient substrate out of Gly, Ala, Ser and Gln in counterflow experiments. Proteoliposomes were loaded with 20mM Hepes/Tris pH7, 100mM NaCl, + 4mM Ala, 4mM Gln, 4mM Ser, and 4mM Gly. Uptake was performed at 30°C in either 20mM Hepes/Tris pH7, 100mM NaCl or 20mM Hepes pH5.2, 100mM NaCl and in the presence of either 500nM [^{3}H]-Ser, [^{3}H]-Gln, [^{3}H]-Ala, or [^{3}H]-Gly. Time points were taken at 25 min. Background was defined as no protein loaded into the proteoliposomes. Error bars represent SEM of duplicate measurements.

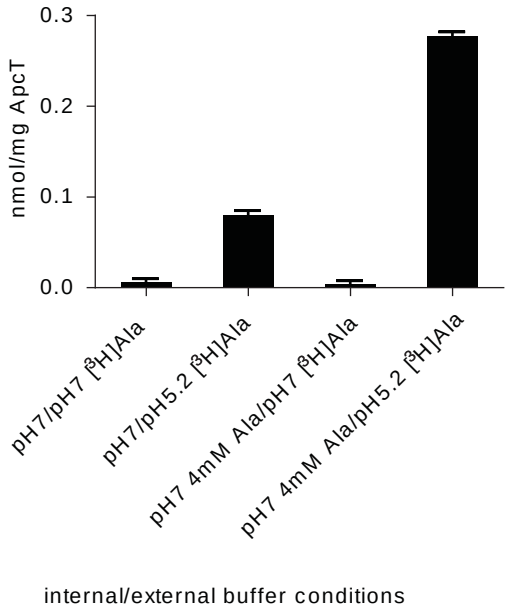

Fig. S4. [^{3}H]-Ala uptake is not dependent on upon substrate counterflow. Proteoliposomes were loaded with 20mM Hepes/Tris pH7 100mM NaCl, +/- 4mM alanine. Uptake was performed at 30°C in either 20mM Hepes/Tris pH7, 100mM NaCl, and 500nM [^{3}H] alanine or 20mM Hepes pH5.2, 100mM NaCl, 500nM [^{3}H] alanine and 10mM of the indicated amino acid. Time points were taken at 25 min. Background was defined as no protein loaded into the proteoliposomes. Error bars represent SEM of triplicate measurements.

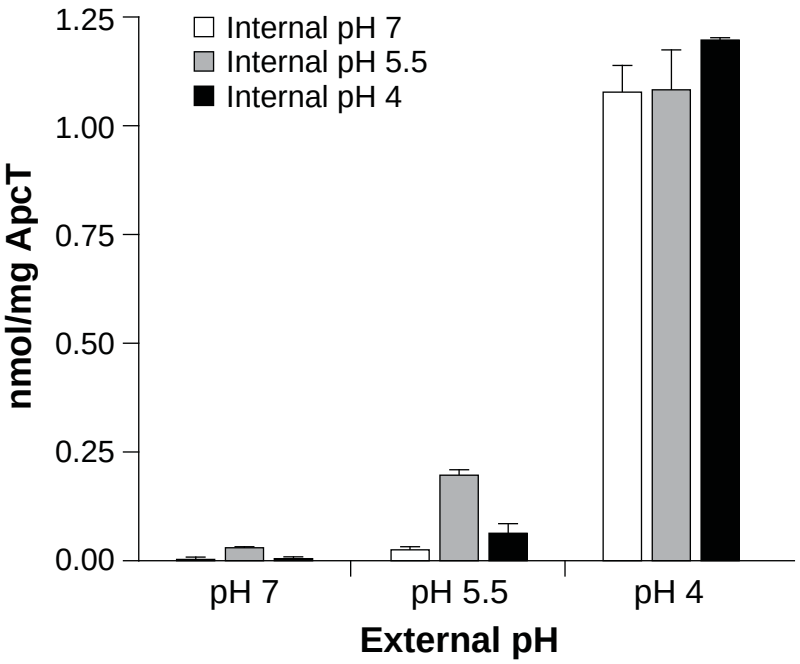

Fig. S5. [^{3}H]-Ala uptake by ApcT is activated at low pH in counterflow experiments. Proteoliposomes were loaded with 100mM NaCl, + 4mM Ala and either 25mM citrate-phosphate buffer pH7, pH5.5, or pH4 (white, grey, and black bars, respectively). Uptake was performed at 30°C in either 25mM citrate-phosphate buffer pH7, pH5.5, or pH4, and in the presence of 100mM NaCl and 500nM L-[^{3}H]alanine. Time points were taken at 20 min.

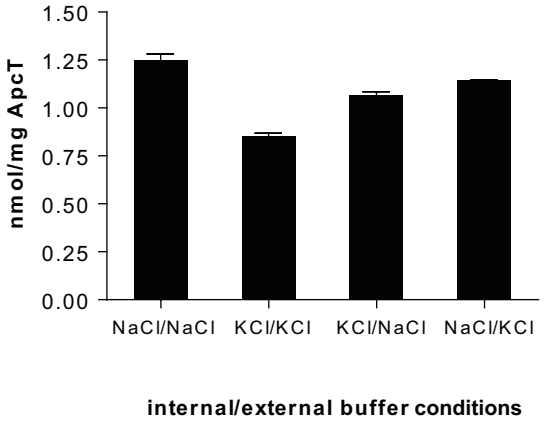

Fig. S6. [^{3}H]-Ala transport by ApcT is not dependent upon sodium or a sodium gradient. Proteoliposomes were loaded with 25mM citrate-Na phosphate buffer pH4, 100mM NaCl, 4mM Ala or 25mM citrate-K phosphate buffer pH4, 100mM KCl, 4mM Ala. Uptake was performed at 30°C in either 25mM citrate-Na phosphate buffer pH4, 100mM NaCl, or 25mM citrate-K phosphate buffer pH4, 100mM KCl, and in the presence of 500nM [^{3}H]alanine. Time points were taken at 20 min. Background was defined as no protein loaded into the proteoliposomes. Error bars represent triplicate measurements.

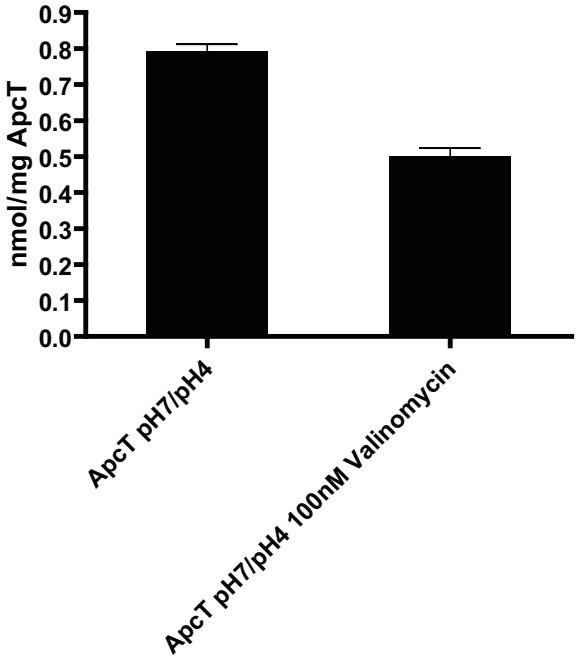

Fig. S7. Effect of valinomycin treatment on [^{3}H]-Ala uptake by ApcT. Proteoliposomes were loaded with 100mM KCl, and 20mM citrate buffer pH7. Uptake was performed at 30°C in 20mM citrate buffer pH4, 100mM KCl, 750nM L-[^{3}H]alanine and in the presence or absence of 100nM valinomycin. Time points were taken at 20 min.

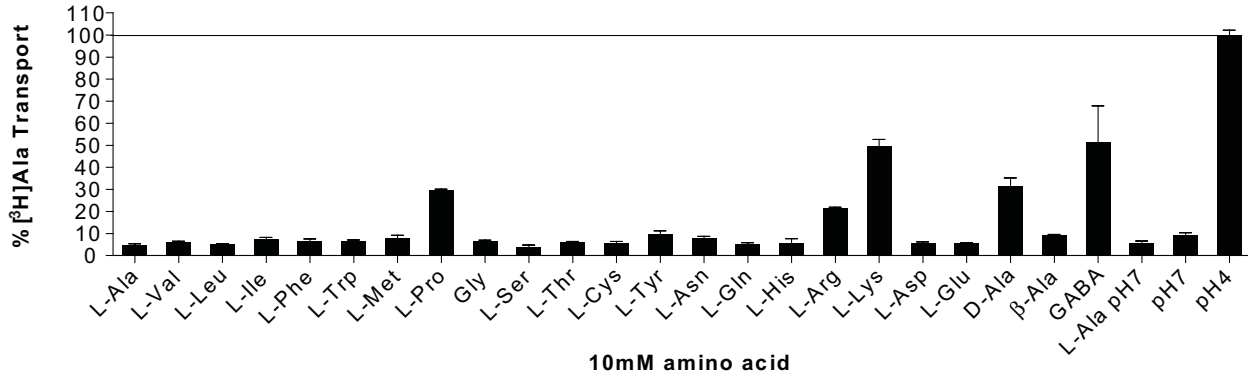

Fig. S8. Inhibition of [^{3}H]Ala transport by cold L-amino acids. Proteoliposomes were loaded with 25mM citrate-phosphate buffer pH4, 100mM NaCl, 4mM Ala. Uptake was performed at 30°C in either 25mM citrate-phosphate buffer pH4 or pH7, and in the presence of 100mM NaCl and 500nM [^{3}H]alanine. Time points were taken at 20 min. Measurements are total [^{3}H] Ala counts.

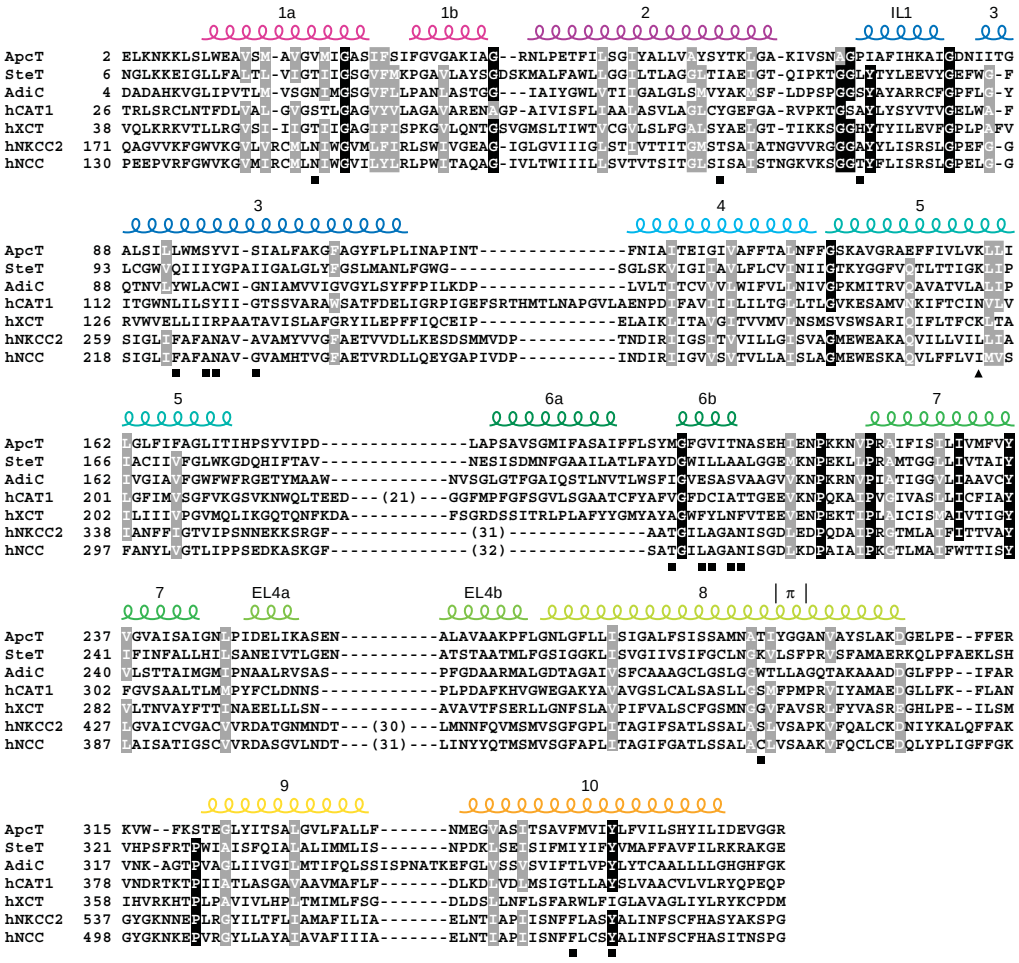

Fig. S9. Amino acid sequence alignment and secondary structure of ApcT.
Amino acid sequence alignment of *M. jannaschii* ApcT (gi|15668789), Ser/Thr exchanger transporter (SteT; gi|81669156), arginine/agmatine antiporter (AdiC; gi|38605621), cationic amino acid transporter (CAT1; gi|4507047), cystine/glutamate transporter (xCT; gi|5668545), NaCl/KCl symporter (NKCC2; gi|134254459), and NaCl symporter (NCC; gi|223634707) generated by PROMALS (http://prodata.swmed.edu/promals3d/promals3d.php) with manual adjustment of the register by one space for xCT sequence between residues 123-124 (TM3) and 161-162. Identical (black) and similar (grey) residues are indicated by shading. α-helices in ApcT are depicted as coils and are colored as in fig. 2. Residues involved in binding of water molecules in the occluded pocket (filled squares) and proton-activated exchange of substrates (K158, filled triangle), are indicated with symbols. For the eukaryotic transporters, residues at the N- and C- termini and between TM5 and TM6a as well as EL4a and EL4b are truncated and the numbers of truncated residues are shown in parentheses.

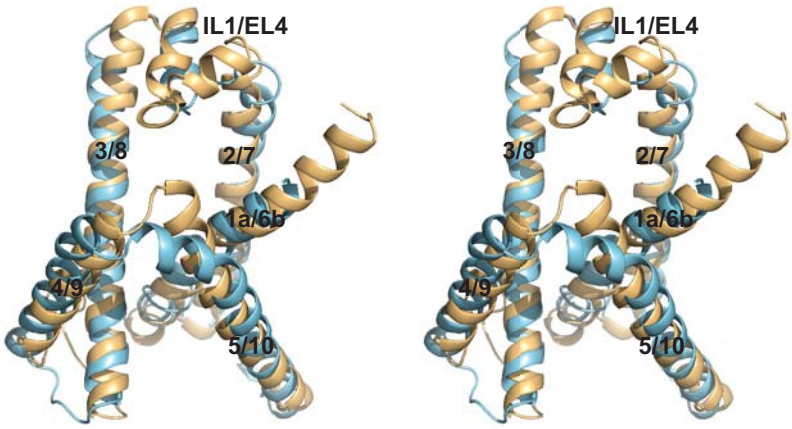

Fig. S10. ApcT has a pseudo 2-fold axis that relates TMs 1-5 and 6-10.
TMs 1-5 and IL1 (cyan) and TMs 6-10 and EL4 (gold) of ApcT are superposed on each other to represent the internal two-fold symmetry in the structure.

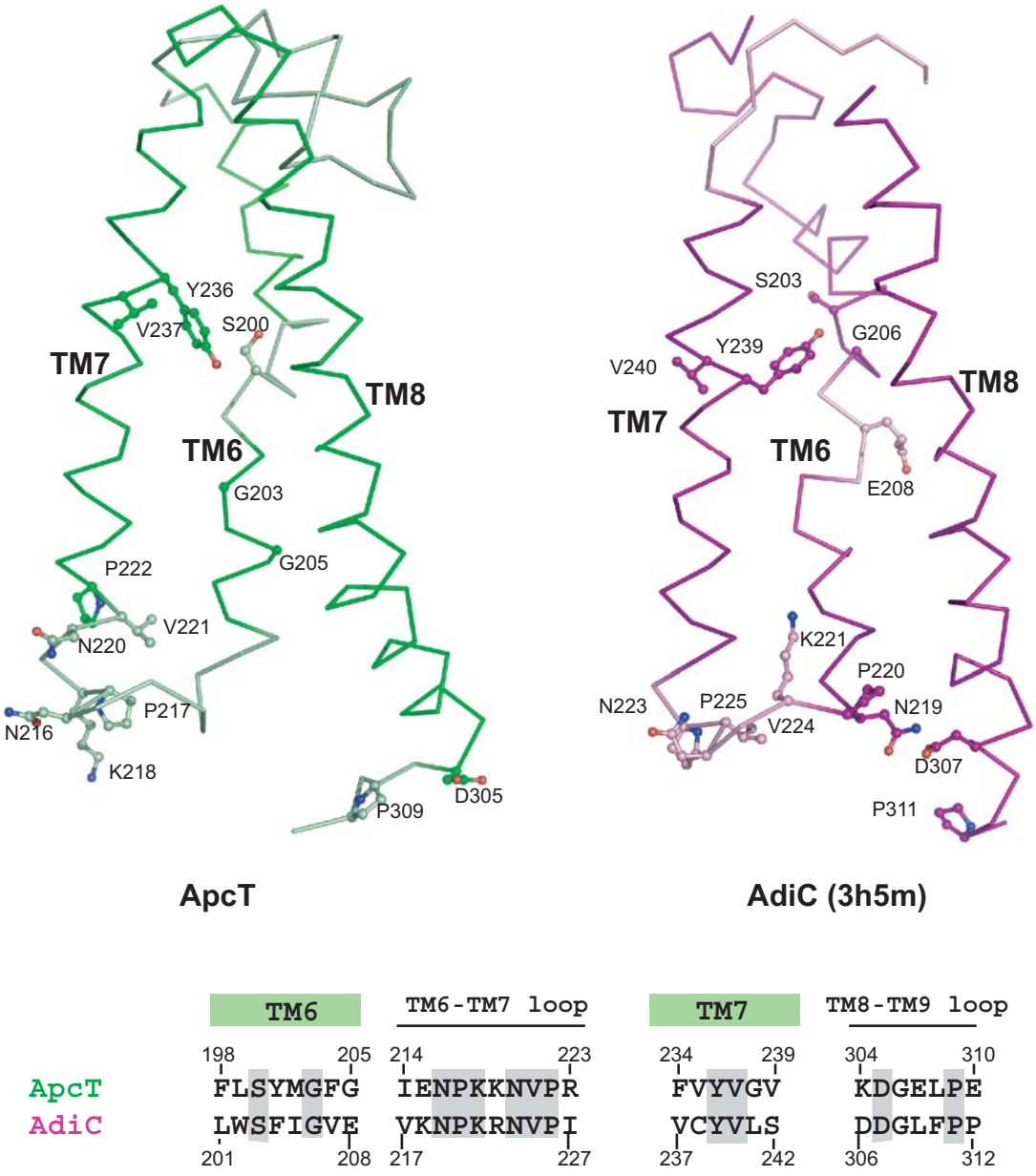

Fig. S11. Structure-based amino acid alignment of ApcT and AdiC (3h5m) do not agree. (A) AdiC structure is off register in correct assignment of amino acids starting from TM5-TM6 loop. ApcT and AdiC structures were superimposed and the relative positions of key conserved residues in TM6 through TM8 are shown as ball and stick models. ApcT is shown in green and AdiC is shown in purple.
(B) Sequence alignment of ApcT and AdiC was generated using PROMALS 3D software. Conserved residues in TM6, TM7 and TM6-TM7 loop and TM8-TM9 loop are highlighted in grey boxes.

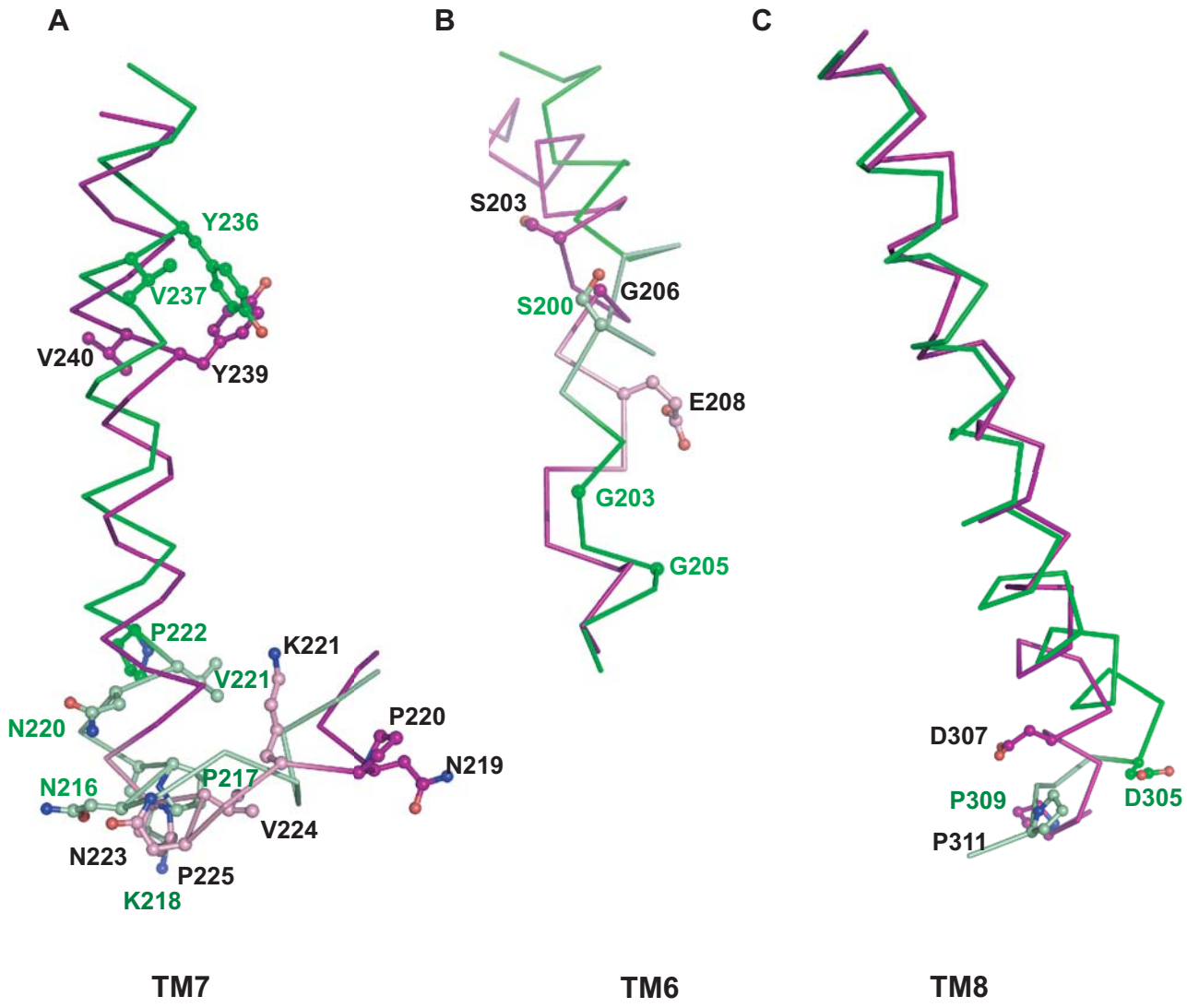

Fig. S12 Structural overlay of TMs 6, 7 and 8 of ApcT and AdiC (3h5m)
ApcT and AdiC (3h5m) structures were superimposed and the overlay of theirs Cα traces in TMs 6, 7 and 8 are shown individually. ApcT is shown in green and AdiC is shown in purple. The relative positions of key conserved residues (shown as ball and stick models) do not overlay. For example, in (A) Y239 of AdiC should overlay with Y236 of ApcT, in (B) E208 of AdiC should approximately align with G205 of ApcT and in (C) D307 of AdiC should align with D305 of ApcT.

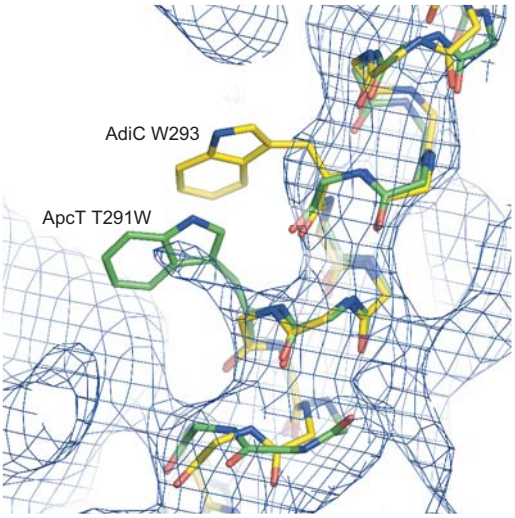

Fig. S13. Superposition of ApcT and AdiC onto electron density map of AdiC (3h5m)
The 2Fo-Fc electron density map (blue mesh) of AdiC was calculated from the PDB-deposited 3H5M structure factors using Phenix and is displayed at 0.4 sigma in Pymol. No structural refinement was done. The superposition of ApcT (green) onto AdiC (yellow) shows that the position of ApcT T291, which aligns with AdiC W293 in sequence alignments, is the correct position of the AdiC W293. This is consistent with W293 being out of register in the structural model 3h5m. The figure shows T291 in ApcT mutated to tryptophan to illustrate the likely position of AdiC W293 and it demonstrates that there is electron density for the side chain at this position.

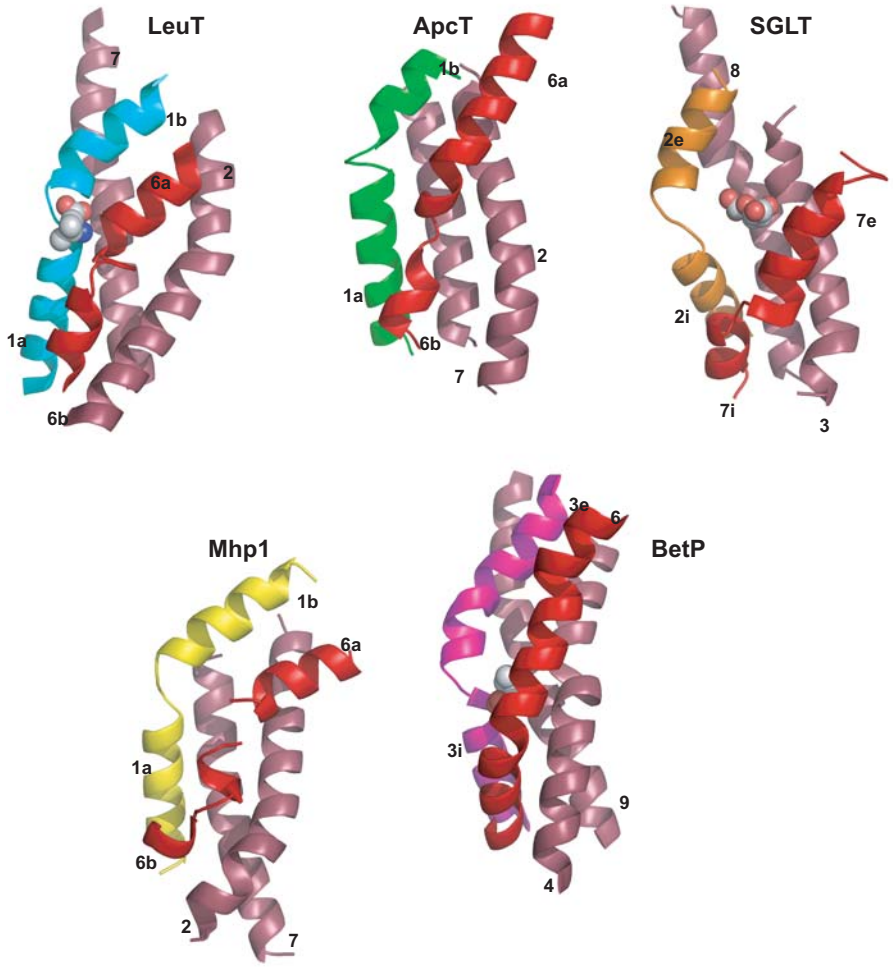

Fig. S14. Helix 'bundle' comparison: LeuT, ApcT, vSGLT, Mhp1 and BetP
The structures of ApcT, SGLT (PDB ID: 3DH4), Mhp1 (2JLN) and BetP (2W8A) were superimposed by the program DaliLite on the structure of LeuT (2A65) using their scaffold helices (TMs 3-5, 8-10 ApcT numbering) and the relative orientations of their bundle helices (TMs 1-2, 6-7) are shown for comparison. TM 6 is shown in red and TMs 2 and 7 are shown in raspberry color for all transporters. TM 1 of LeuT, ApcT, SGLT, Mhp1 and BetP are shown in cyan, green, orange, yellow and magenta, respectively. The substartes leucine (bound to LeuT), galactose (bound to SGLT) and betaine (bound to BetP) are represented as sphere models.

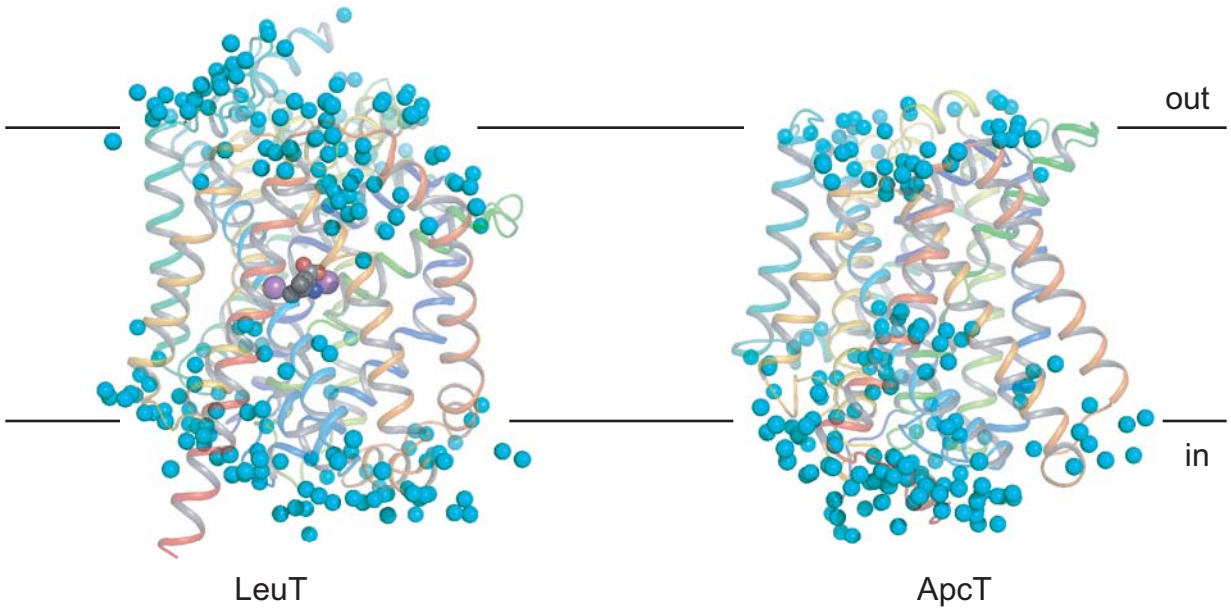

Fig. S15. Comparison of water distribution in LeuT and ApcT structure suggests an inward facing conformation for ApcT.
Water molecules in the structures of LeuT (2A65; left) and ApcT (right) are shown as spheres in cyan color. Leucine bound to LeuT is shown as sphere model with carbon, nitrogen and oxygen atoms colored in grey, blue and red respectively. The two Na ions bound to LeuT are shown in violet.

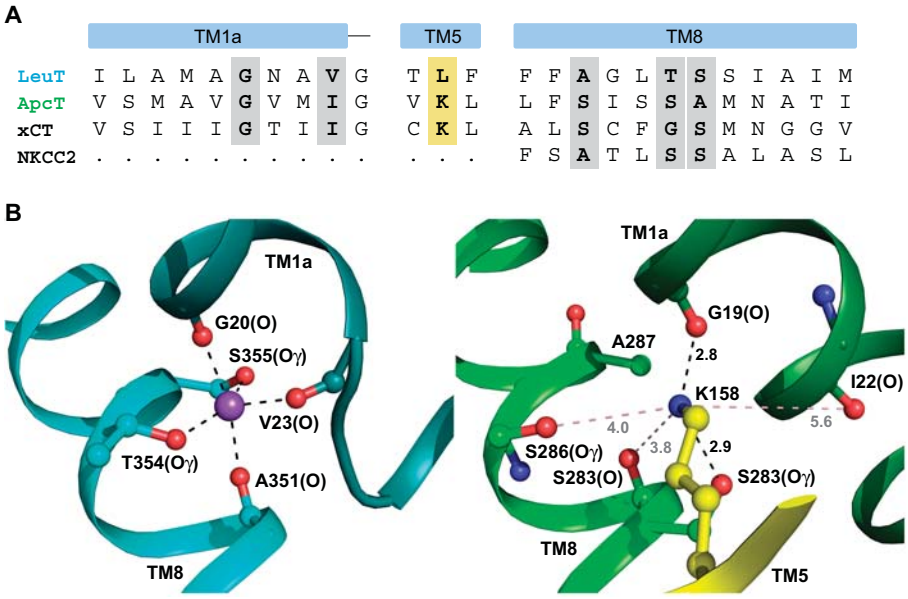

Fig. S16. K158 site in ApcT superposes in Na2 site in LeuT
(A) Amino acid sequence alignment and secondary structure assignment of ApcT, indicating conserved features in LeuT, human xCT and human NKCC2 surrounding Lys158 in the structure of ApcT. The grey boxes indicate residues that line up with critical Na2 binding residues in LeuT. Yellow box indicates residues that line up with Lys158 of ApcT. The alignment for LeuT with ApcT and xCT was generated by PROMALS 3D. Alignment of ApcT with the orthologues of human NKCC2 was generated separately and the residues corresponding to TM8 of ApcT were manually added to the above alignment. Dotted lines indicate regions where the alignment is poor.
(B) The ammonium group of Lys158 in ApcT occupies a similar position as Na2 site in LeuT. Left panel represents the helices TM1a and TM8 and the key interacting residues in the Na2 site of LeuT. Right panel represents helices TM1a, TM5 and TM8 and the key residues surrounding the ammonium group of Lys158 in ApcT. Black dashed lines indicate hydrogen bonds.
Pink dashed lines indicate hydrogen bonds that are likely to form upon a conformational change following the protonation of Lys158. Numerical values indicate bond distances in Å.

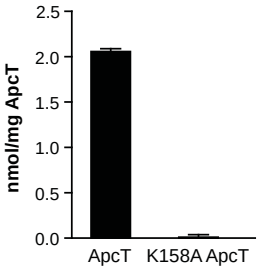

Fig. S17. K158A mutation abolishes L-alanine exchange into lipid vesicles by ApcT. ApcT and K158A ApcT proteoliposomes were loaded with pH7.0 buffer and 4mM L-Ala. Uptake was performed at 30°C in 20mM Citric Acid-NaOH pH4.0 buffer and in the presence of 100mM NaCl and 500nM L-[^{3}H]alanine. Time points were taken at 20 min. Background was defined as no protein loaded into the proteoliposomes. Error bars represent SEM of triplicate measurements.

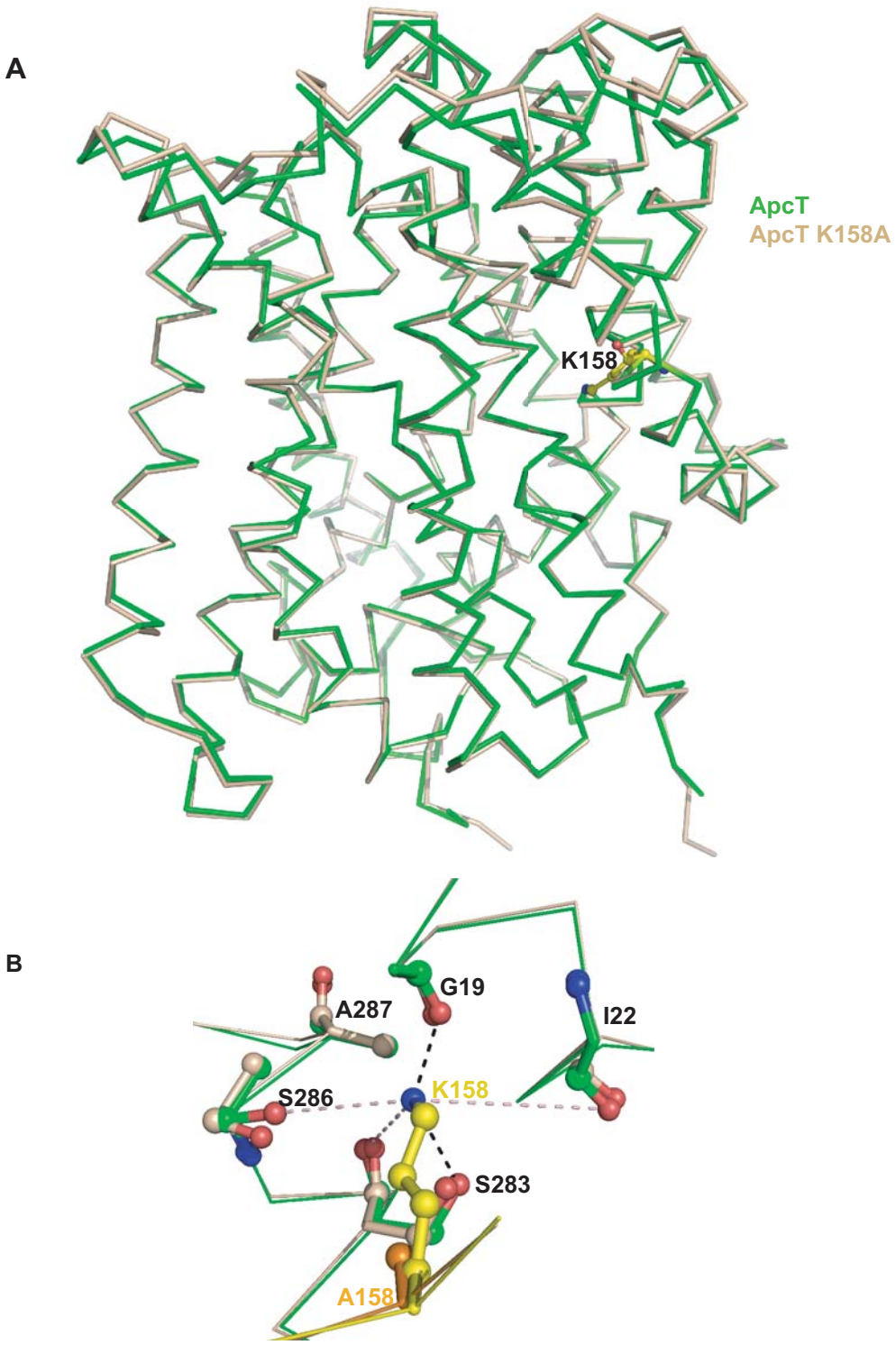

Fig. S18 ApcT K158A adopts a similar conformation as WT ApcT
(A) Structural superposition of the crystal structures of ApcT and ApcT K158A. The two structures can be superposed with a RMSD of ~0.4Å for their Cα atoms. ApcT structure is shown in green color and ApcT K158A structure is shown in light brown color. Lys158 in ApcT is shown as a ball and stick model to show its position in the overall structure.
(B) Close-up view of Lys158 (or Ala158) in the superposed ApcT and ApcT K158A structures. Mutation of Lys to Ala does not show any significant perturbation in the structure of the key surrounding residues. N and O atoms are colored blue and red, respectively.

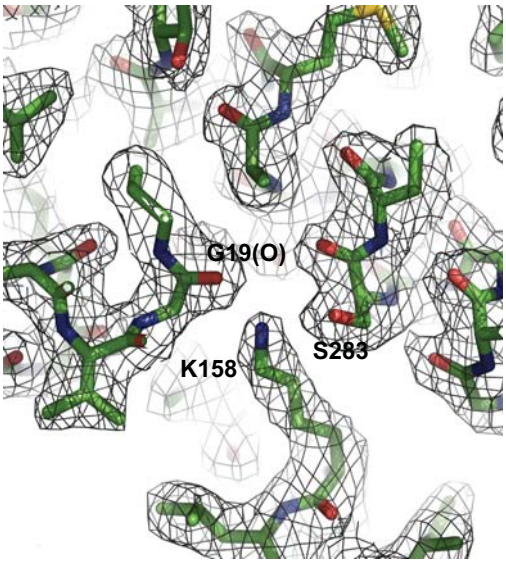

Fig. S19. 2fo-fc electron density map (contoured at 1.0 sigma) showing Lys158 and residues in TMs 1 and 8.

Table S1: Mammalian Cell Amino Acid Transport Systems

Family[a]	HUGO[b]	Alternative name(s)	Mammalian transport system[c]
Heterodimeric Amino Acid Transporters (HATs)	SLC7A5	L-type neutral amino acid transporter, LAT1	L
	SLC7A6	y+LAT2	y+L
	SLC7A7	y+LAT1	y+L
	SLC7A8	L-type neutral amino acid transporter, LAT2	L
	SLC7A9	BAT1, $b^{o,+}AT$	$b^{o,+}$
	SLC7A10	asc-1	asc
	SLC7A11	cystine/glutamate transporter, xCT	X^-_c
	SLC7A13	AGT1	
Cationic Amino Acid Transporters (CATs)	SLC7A1	Cationic amino acid transporter 1, CAT1	y+
	SLC7A2	CAT2	y+
	SLC7A3	CAT3	y+
	SLC7A4	CAT4	
Cation-Chloride Co-transporters (CCCs)	SLC12A1	NaCl/KCl symporter, NKCC2	
	SLC12A2	NKCC1	
	SLC12A3	NaCl symporter, NCC	
	SLC12A4	KCl symporter, KCC1	
	SLC12A5	KCC2	
	SLC12A6	KCC3	
	SLC12A7	KCC4	
Vesicular Inhibitory Amino Acid Transporter (VIAAT)	SLC32A1	GABA vesicular transporter, VIAAT	
System A/N Amino Acid Transporters (SNATs)	SLC38A1	Sodium-coupled neutral amino acid transporter, SNAT1	A
	SLC38A2	SNAT2	A
	SLC38A4	SNAT4	A
	SLC38A3	SNAT3	N
	SLC38A5	SNAT5	N
	SLC38A6	SNAT6	
Proton-Coupled Amino Acid Transporters (PATs)	SLC36A1	proton-coupled amino acid transporter, PAT1	
	SLC36A2	PAT2	
	SLC36A3	PAT3	
	SLC36A4	PAT4	

[a]Family designations are classed according to the TC classification (www.tcdb.org).
[b]Nomenclature designated in the SLC (solute carrier) series according to the Human Gene (HUGO) Nomenclature Committee Database (http://www.genenames.org).
[c]Designations for the Mammalian Amino Acid Transport system have been reviewed elsewhere (Wagner CA et al. 2001, Chillaron J et al. 2001, Mackenzie B and Erickson JD 2004).
System A: widely expressed, cotransports Na^+ with mainly neutral amino acids with broad selectivity including *N*-methyl amino acids.
System asc: specifically transports small neutral amino acids.
System $b^{o,+}$: widely expressed, transports dibasic and some neutral amino acids.
System L: widely expressed, transports neutral-branched chains and aromatic amino acids.
System N: cotransports Na^+ with glutamine and asparagine (and occasionally histidine) with the countertransport of protons.
System X^-_c: glutamate-cystine exchanger.
System y+: widely expressed, transports cationic and zwitterionic amino acids.
System y+L: expressed mainly in erythrocytes and placenta, transports basic amino acids without Na^+, but cotransports neutral amino acids with Na^+.

Table S2: ApcT +/- Fab Data Collection Statistics

	ApcT	**ApcT + 7F11 Fab**	**SeMet ApcT + 7F11 Fab**	**ApcT K158A + 7F11 Fab**
Beamline	ALS 8.2.2	ALS 8.2.1	ALS 8.2.1	ALS 5.0.2
Wavelength (Å)	0.9793	1.0000	0.9793	1.0332
Space Group	C2	C2	$P2_1$	$P2_1$
Cell Dimensions				
a, b, c (Å)	113.5, 99.5, 72.7	148.4, 45.9, 158.1	46.0, 111.2, 115.0	46.0, 111.2, 115.7
β (º)	117.7	97.8	91.6	90.9
Resolution (Å) [a]	50-2.35 (2.43-2.35)	50-2.50 (2.59-2.50)	50-2.90 (3.00-2.90)	50-2.60 (2.69-2.60)
R_{merge} (%)[b]	10.6 (71.5)	5.2 (30.2)	8.0 (54.4)	8.7 (33.5)
$I/\sigma I$	18.6 (2.1)	24.3 (2.1)	20.7 (2.2)	17.4 (3.0)
Completeness (%)	99.9 (99.3)	93.5 (70.3)	98.4 (96.3)	99.6 (96.8)
Redundancy	7.4 (7.1)	3.2 (2.1)	5.6 (5.4)	4.4 (3.9)

[a] Number in parentheses represents statistics for data in the highest resolution shell.

[b] $R_{merge} = \sum_{hkl}\sum_i |I_i(hkl)_i - \langle I(hkl)\rangle| / \sum_{hkl}\sum_i I_i(hkl)$.

Table S3: ApcT +/- Fab Refinement Statistics

	ApcT	**ApcT – 7F11 Fab**	**ApcT K158A – 7F11 Fab**
Resolution (Å)	50-2.35	50-2.50	50-2.60
No. reflections	28918	34113	34243
R_{work}[a]/R_{free}[b] (%)	20.3 (23.4)	24.6 (29.5)	26.1 (30.8)
No. atoms			
Protein	3344	6714	6719
Water	176	151	118
Other	71		
B-factors (Å^2)			
Overall	38.3	50.9	56.5
Protein	37.3	51.1	56.7
Water	47.0	44.6	48.6
Other	64.0		
RMSD			
Bond lengths (Å)	0.009	0.006	0.007
Bond angles (°)	1.06	0.94	1.01
Ramachandran Plot[c]	97.5/2.5/0	96.2/3.8/0	93.1/5.4/1.5

[a] $R_{work} = \sum||F_o| - |F_c||/\sum|F_o|$, where F_o and F_c are the observed and calculated structure factor amplitudes, respectively.

[b] R_{free} is equivalent to Rwork for a 5% subset of reflections excluded from refinement.

[c] Percentage of amino acids in the favored, allowed, and disallowed regions of the Ramachandran plot, respectively.

Table S4: **The degree of openness or closeness of transporter gates.**

	Angular difference of TMs 1a with reference to LeuT (θ opening to in)	**Angular difference of TMs 1b with reference to LeuT** (θ opening to out)
ApcT	-21.77	-11.33*
vSGLT	-41.36	20.81
Mhp1	-19.35	-13.24
BetP	-29.76	13.79

Interhelical angles were computed using the interhlx program as described in methods. The angle of rotation (θ) required to orient (N->C) TMs 1a or 1b of ApcT, vSGLT, Mhp1 or BetP on that of LeuT is shown with a clockwise rotation giving a positive value and a counterclockwise rotation giving a negative value. The more negative θ is for TM1a, the more open the gate is to the intracellular side compared to LeuT. The more positive θ is for TM1b, the more closed the gate is to the extracellular side compared to LeuT. *The angular difference measured for TM1b in ApcT is not reliable due to its shorter length compared to other transporters.